Numerical Solution of Space Shuttle Orbiter Flowfield

John V. Rakich*
NASA Ames Research Center, Moffett Field, California
and
Ethiraj Venkatapathy,† J. C. Tannehill,‡ and Dinesh Prabhu§
Iowa State University, Ames, Iowa

The supersonic viscous laminar flow around the Space Shuttle Orbiter forebody has been computed with a parabolized Navier-Stokes code using a generalized coordinate transformation. The initial solution for the nose part of the Orbiter was obtained with a three-dimensional time-dependent Navier-Stokes solver. It was necessary to employ a wind-axis oriented coordinate system to obtain the initial solution with the time-dependent code. The generalized PNS technique was then used to march the solution downstream from the given initial data surface. An algebraic grid generation scheme was employed which accurately describes the body shape by clustering points at the wing tip and at the wing-body juncture. The computed heat-transfer coefficients, pressure coefficients, and shock shapes are compared with the available experimental data for 0 and 30 deg angle of attack.

Nomenclature

A_i, B_i = parameters controlling clustering of grid points in circumferential direction
C_p = pressure coefficient
$\bar{E}, \bar{F}, \bar{G}$ = flux vectors of the PNS equations written in strong conservation-law form for the ξ, η, ζ coordinates
$\bar{E}^*$ = flux vector $\bar{E}$ with fraction $(1-\omega)\bar{P}$ of the pressure omitted
h = heat-transfer coefficient
$\boldsymbol{i}, \boldsymbol{j}, \boldsymbol{k}$ = unit vectors in x, y, z directions
L = total length
M = Mach number
$\boldsymbol{n}$ = unit vector in η direction
p = pressure
$\bar{P}$ = vector representing a fraction $(1-\omega)p$ of the pressure
Re_L = Reynolds number based on L and freestream conditions
s = stretch function
s = arc length along body in ζ direction
T = temperature
$\bar{U}$ = dependent variable vector of the unsteady Navier-Stokes equations written in strong conservation-law form for the ξ, η, ζ coordinates
x, y, z = Cartesian coordinates
α = angle of attack
β = parameter controlling clustering of grid points between body and shock
δ = shock standoff distance along η direction
θ_1, θ_2 = parameters controlling type of difference scheme
ξ, η, ζ = generalized curvilinear coordinates
ϕ = circumferential angle
ω = fraction of pressure gradient term which makes PNS equations formally parabolic

Subscripts and Superscripts

i, j, k = indices labeling grid points along ξ, η, ζ coordinates
ref = reference value
stag = stagnation point value
w = wall value
∞ = freestream value

Introduction

RECENTLY great interest has been shown in using the parabolized Navier-Stokes (PNS) equations to calculate the viscous supersonic flow around bodies at incidence. Early efforts by Rubin and Lin[1,2] and Lubard and Helliwell[3] set the pattern for current research work. Although the earlier methods were successful in calculating the viscous flow around sharp and blunt-nose bodies,[3-5] poor reliability and efficiency led to the search for more efficient and stable schemes, resulting in fully implicit noniterative marching schemes, developed by Vigneron et al.[6] and Schiff and Steger.[7] These methods were restricted by marching planes that are normal to the marching axis. This limitation was removed by the present authors by generalizing the transformation and the marching procedure.[8]

The calculation of the complete inviscid-viscous flow around the Space Shuttle Orbiter with a single code has been the aim of recent research efforts. Although inviscid flow solutions[9-14] and other solution techniques that couple the inviscid solution with the matching boundary-layer analysis[15,16] have resulted in limited solutions for the windward side of Shuttle-like bodies, they have failed in general to predict the correct solution on the lee side and near the wing root region. On the other hand, PNS solvers have shown great promise in solving the complex flowfield around Shuttle-like bodies.[17,18]

The present generalized PNS solver is ideally suited for the complex flow that develops around the sharp leading edge and in the vicinity of the wing-body juncture of the Orbiter. Although this generalized marching procedure was used to obtain the solution of the flow around a blunt delta wing at large angles of incidence,[8] that flow did not provide a complete test of the method. The full capabilities of the

Presented as Paper 82-0028 at the AIAA 20th Aerospace Sciences Meeting, Orlando, Fla., Jan. 11-14, 1982; submitted Feb. 5, 1982; revision received March 10, 1983.

*Research Scientist. Associate Fellow AIAA.
†Research Assistant, Department of Aerospace Engineering and Computational Fluid Dynamics Institute; presently, PEDA Corp., Palo Alto, Calif. Member AIAA.
‡Professor, Department of Aerospace Engineering and Computational Fluid Dynamics Institute. Associate Fellow AIAA.
§Research Assistant, Department of Aerospace Engineering and Computational Fluid Dynamics Institute. Member AIAA.

generalized PNS code are used in the present problem. The main advantages of the present code are that it can accept the initial solution on any starting data surface and it also will allow the marching to proceed from one solution to another without any restriction on these solution surfaces. The only condition that must be met is that the velocity component normal to the solution surface must be supersonic outside the boundary layer.

The above salient features of the generalized PNS code were of great help in solving the flow around the forward half of the Space Shuttle Orbiter at angles of incidence up to 30 deg for different freestream Mach numbers. The body geometry routine properly models the wing and the wing-body juncture regions. Results for the different cases are compared with available experimental data for surface pressure, shock profile, and heat-transfer coefficients.

Parabolized Navier-Stokes Equations

The so-called "parabolized" Navier-Stokes (PNS) equations are obtained from the complete Navier-Stokes equations by neglecting the unsteady terms and the streamwise viscous derivative terms. The resulting equations can be written in the following vector form:

$$\frac{\partial \bar{E}}{\partial \xi} + \frac{\partial \bar{F}}{\partial \eta} + \frac{\partial \bar{G}}{\partial \zeta} = 0 \tag{1}$$

for a generalized curvilinear coordinate system. Complete details of all the terms involved in Eq. (1) are given in Ref. 8. The above system of equations is parabolic in the ξ direction if the inviscid region of the flowfield is completely supersonic, if there is no streamwise flow separation within the domain of interest, and if the pressure gradient near the wall is properly treated. Due to the upstream influence that feeds through the thin subsonic layer next to the body, the solution of the above system of equations becomes an ill-posed,[19] initial boundary-value problem if the pressure gradient term $\partial p/\partial \xi$ is represented exactly. The PNS equations allow departure solutions if this pressure gradient term is not modified.

A novel way to avoid the departure associated with the pressure gradient term was proposed by Vigneron et al.,[6] whose technique is utilized in the present formulation. According to Vigneron's eigenvalue analysis the equations are formally parabolic if a fraction of the pressure gradient term, $\omega \partial p/\partial \xi$, is retained in the subsonic layer and the remaining part of the pressure gradient term is either neglected or approximated by a backward difference. The "sublayer" approximation technique originally proposed by Rubin and Lin,[1] and later modified by Schiff and Steger,[7] is a subset of the technique proposed by Vigneron. Using Vigneron's pressure gradient approximation, the governing equations are

$$\frac{\partial \bar{E}^*}{\partial \xi} + \frac{\partial \bar{P}}{\partial \xi} + \frac{\partial \bar{F}}{\partial \eta} + \frac{\partial \bar{G}}{\partial \zeta} = 0 \tag{2}$$

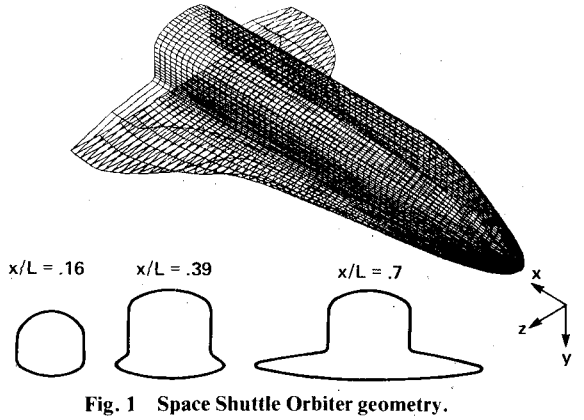

Fig. 1 Space Shuttle Orbiter geometry.

The generalized PNS solver uses the above set of equations to solve the viscous flow around bodies as an initial boundary-value problem.

Finite Difference Algorithm

The PNS equations in the generalized coordinate system are solved using an efficient, noniterative, implicit, approximate factorization finite difference algorithm. The present algorithm is a direct adaptation of the one used by Vigneron et al.,[6] which is closely related to the schemes developed by Lindemuth and Killeen,[20] McDonald and Briley,[21] and Beam and Warming[22] to initially solve the unsteady Navier-Stokes equations. The finite difference algorithm is

$$\left[\frac{\partial \bar{E}^*}{\partial \bar{U}} + \frac{\theta_1}{1+\theta_2}\Delta\xi \frac{\partial}{\partial \zeta}\left(\frac{\partial \bar{G}}{\partial \bar{U}}\right)\right]\left(\frac{\partial \bar{E}^*}{\partial \bar{U}}\right)^{-1} \times \left[\frac{\partial \bar{E}^*}{\partial \bar{U}} + \frac{\theta_1}{1+\theta_2}\Delta\xi \frac{\partial}{\partial \eta}\left(\frac{\partial \bar{F}}{\partial \bar{U}}\right)\right]\Delta^i \bar{U}$$
$$= \frac{-\Delta\xi}{1+\theta_2}\left(\frac{\partial \bar{F}}{\partial \eta} + \frac{\partial \bar{G}}{\partial \zeta}\right)^i + \frac{\theta_2}{1+\theta_2}\Delta^{i-1}\bar{E} - \Delta^i \bar{P}$$
$$-\Delta\xi\left(\frac{\partial \bar{E}^*}{\partial \xi}\right)^i_{\bar{U}} - \frac{\theta_1}{1+\theta_2}(\Delta\xi)^2\left[\frac{\partial}{\partial \eta}\left(\frac{\partial \bar{F}}{\partial \xi}\right)^i_{\bar{U}} + \frac{\partial}{\partial \zeta}\left(\frac{\partial \bar{G}}{\partial \xi}\right)^i_{\bar{U}}\right] \tag{3}$$

where

$$\Delta^i \bar{U} = \bar{U}^{i+1} - \bar{U}^i \tag{4}$$

The inviscid and viscous Jacobian terms are given in Ref. 23. Second-order central difference expressions are used to evaluate the η and ζ derivative quantities. The Euler implicit scheme ($\theta_1 = 1$, $\theta_2 = 0$), which has first-order accuracy in the marching direction, was used for all of the present computations. Further details of the algorithm implementation are given in Ref. 8.

Boundary Conditions

In the present code the outer shock boundary is fitted using a shock-fitting procedure similar to that of Thomas et al.[24] At the body boundary the velocity components are set to zero and the normal pressure gradient term is assumed to be zero. For an isothermal wall boundary, the specified body temperature determines the density and thus all of the flow quantities are known at the body. For an adiabatic wall, the normal total temperature gradient is set to zero. By imposing reflection boundary conditions about the plane of symmetry, flow symmetry is maintained for zero yaw angle. The body boundary condition and the reflection boundary condition are imposed implicitly. The shock boundary condition is an explicit boundary condition which may place limitations on the maximum step size, however, the body boundary usually limits the step size.

Shuttle Geometry

The Shuttle surface coordinates are obtained with the geometry package of Rakich and Kutler.[9] This geometry

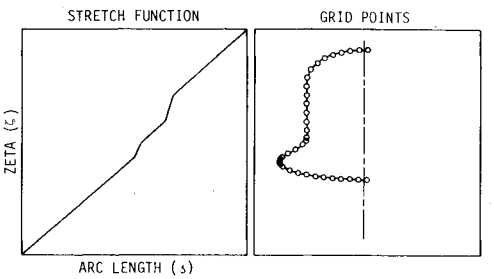

Fig. 2 Stretch function and grid points.

package reproduces the Shuttle geometry exactly at 11 different axial locations, and intermediate to these locations, interpolation polynomials are used to produce a smooth geometry that models the actual Shuttle geometry very closely. Figure 1 shows three-dimensional and cross-sectional views of the Space Shuttle Orbiter obtained with the above geometry package. Complete details of the geometry package used in this study are given in Refs. 25 and 26. Note that the present Shuttle geometry does not include the canopy or the vertical tail region.

Grid Generation

The PNS method requires the grid to be generated at every ξ station, which demands the use of a fast grid generation scheme. Numerous grid generation methods are available in the literature, but these schemes usually require the solution of a partial differential equation.

A simple and efficient algebraic grid generation scheme is used in the present study that allows the grid points on the body and the shock curves to be clustered in regions of high curvature. This is accomplished in the following manner. The inner body boundary curve or the outer shock boundary curve is parametrized by a nondimensional arc length parameter δ in the physical plane. In the computational plane, the corresponding parameter that represents the inner or outer boundary curve is ζ. The relationship between ζ and δ, which is referred to as the "stretch function," maps the equispaced grid points in the computational region into the non-equispaced grid points on the inner or outer boundary curve in the physical plane. Initially it seemed appropriate to cluster the grid points in regions of high curvature. Unfortunately, this approach does not allow the user to choose the desired clustering and yields unrealistic grids. However, a stretch function can be written in the following form which permits the user to tailor the clustering to the requirements of each flowfield.

$$\left(\frac{\partial\zeta}{\partial\delta}\right)_j = A_1\left\{1+\tanh\left[\frac{(\delta_j-\delta_1)}{B_1}\right]\right\}+A_2\left\{1+\tanh\left[\frac{(\delta)_j-\delta_2}{B_2}\right]\right\} \tag{5}$$

where A_1, A_2, B_1, and B_2 are user-specified constants and δ_1 and δ_2 are the arc length values corresponding to locations where clustering is required. Depending on the sign and magnitude of A_1 and A_2 the above stretch function either clusters the grid points closer to one another or stretches them away at the corresponding δ_1 and δ_2 arc length locations. The relationship between δ and ζ is determined by numerically integrating Eq. (5). This relationship, coupled with the fact that the grid points are equispaced in the computational plane, determines the location of the grid points in the physical plane.

Figure 2 shows the clustered grid points for the Orbiter geometry and the corresponding stretch function that was used to cluster the grid points. The grid generation is accomplished using the above stretch-function approach in three steps.

1) The grid points on the inner body boundary curve are located using the algebraic stretch-function approach.

2) The shock boundary curve is determined completely from the known solution at the previous station. Hence the shock boundary grid points are determined from the user-prescribed solution surface orientation. The grid points on the shock boundary can be reclustered, if required, using the stretch-function approach.

3) Interior grid points are located along the straight line rays that connect the appropriate body and shock boundary points. An algebraic stretch function[6] clusters the grid points along each of the rays near the body surface in order to resolve the viscous region properly.

The preceding steps determine all of the grid points in the physical plane. The interior grid points in the physical plane are related to the body grid points as follows:

$$\begin{aligned} x(j,k) &= x_w(j)+\delta(j)s(k)\,[\boldsymbol{n}(j)\cdot\boldsymbol{i}] \\ y(j,k) &= y_w(j)+\delta(j)s(k)\,[\boldsymbol{n}(j)\cdot\boldsymbol{j}] \\ z(j,k) &= z_w(j)+\delta(j)s(k)\,[\boldsymbol{n}(j)\cdot\boldsymbol{k}] \end{aligned} \tag{6}$$

where $\delta(j)$ is the shock standoff distance measured along the rays that emanate from the jth body point with direction cosines $[\boldsymbol{n}(j)\cdot\boldsymbol{i}]$, $[\boldsymbol{n}(j)\cdot\boldsymbol{j}]$, and $[\boldsymbol{n}(j)\cdot\boldsymbol{k}]$, and $s(k)$ is the stretch function that clusters grid points along these rays. The stretch function $s(k)$ is given by

$$s(k) = 1-\beta\left[\left(\frac{\beta+1}{\beta-1}\right)^{\eta}-1\right]\Big/\left[1+\left(\frac{\beta+1}{\beta-1}\right)^{\eta}\right] \tag{7}$$

where β is a parameter that controls the clustering. The grid point location in the computational plane is determined by the following relationships:

$$\begin{aligned} \eta &= (k-1)\,\Delta\eta, & \Delta\eta &= \frac{1}{NK-1} \\ \zeta &= (j-1)\,\Delta\zeta, & \Delta\zeta &= \frac{1}{NJ-1} \end{aligned} \tag{8}$$

where NK is the number of grid points between the body and shock, and k is an integer parameter that varies from $k=1$ at the shock to $k=NK$ at the body. NJ is the number of grid points around the body and j is an integer parameter that varies from $j=1$ on the wind side to $j=NJ$ on the lee side.

Once the location of all the grid points is known both in the physical and the computational domains, the geometric metric quantities and the Jacobian of the transformation are computed by finite difference approximations.[8] The Jacobian and the metric quantities are first-order accurate in ξ and second-order accurate in ζ and η. This is consistent with the difference scheme used in the present study.

Solution Surface Orientation

In all previous computations with the generalized PNS code, the solution surfaces were always planes normal to either the x axis or some other line. In the present study, the initial solution surface obtained from the blunt-body code is a skewed surface. Since the present formulation does not restrict the solution surface in any manner, these surfaces can be generated based on local flow conditions best suited for PNS marching. The proper choice of the orientation of the solution surfaces is determined by the appropriate direction of marching. In effect, the user can control the direction of marching by specifying the orientation of the solution surface at each ξ station. In the present study, the solution surfaces are advanced from the prescribed initial solution surface to a solution surface normal to the x axis at a specified x location. This is accomplished by independently changing the orientation of the vectors that describe the body grid points and the vectors that connect the body and shock grid points. The marching step size becomes different for each grid point in the physical plane. Once the solution surface has become an axis-normal plane, it is maintained axis normal in the present study. Figure 3 shows the solution surfaces at different ξ stations.

Blunt-Nose Solution and Initial Conditions

The PNS code requires a starting solution on an initial data surface where the inviscid flow is supersonic. The presence of an embedded subsonic region in the blunt-nose region requires the use of an axisymmetric or three-dimensional time-dependent Navier-Stokes code for finding the blunt-nose solution. The three-dimensional blunt-body code originally developed

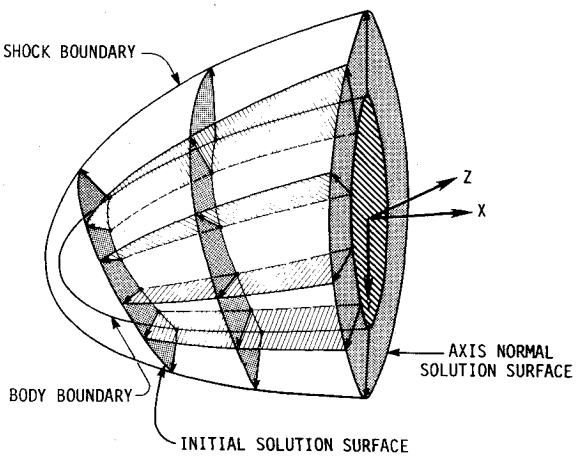

Fig. 3 Solution surface orientation.

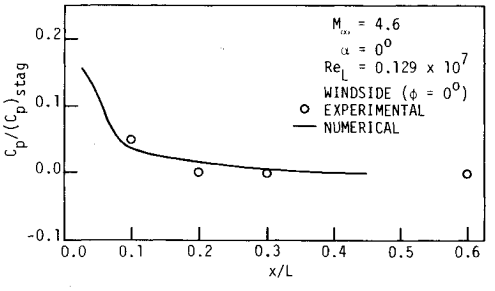

Fig. 4 Comparison of windside ($\phi = 0$ deg) wall pressure.

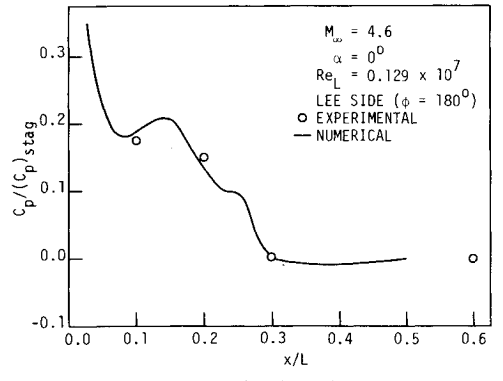

Fig. 5 Comparison of leeside ($\phi = 180$ deg) wall pressure.

by Kutler et al.,[27] and later modified by Rizk et al.,[28] is used to obtain the starting solution for the PNS code.

The blunt-body code requires an initial solution or an approximate shock shape. From the experimentally available shock shapes on the wind and lee sides an approximate shock shape was constructed for the 30-deg angle-of-attack case. It was found that the viscous solution converged in the wind-axis coordinate system, but the solution diverged in the body-axis coordinate system. The solution divergence in the body-axis system is due to the boundary condition procedure on the x axis of this blunt-body code, which is a singular line of the coordinate system. The wind-axis system eliminated the problem because it corresponds closely with the flow stagnation line, thus reducing the error in the boundary condition. Another advantage of the wind-axis system is that the computational domain corresponds more closely with the region of subsonic flow, eliminating unnecessary grid points in the supersonic region. A similar approach was taken by Rizzi and Bailey.[29]

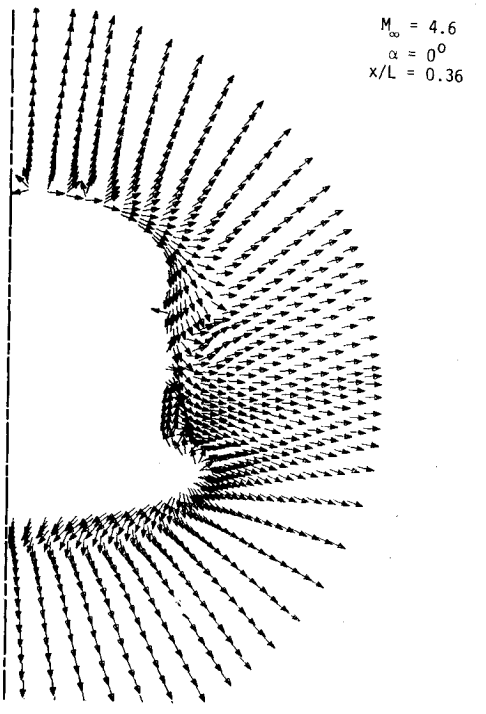

Fig. 6 Cross-flow velocity vector directions at $x/L = 0.36$.

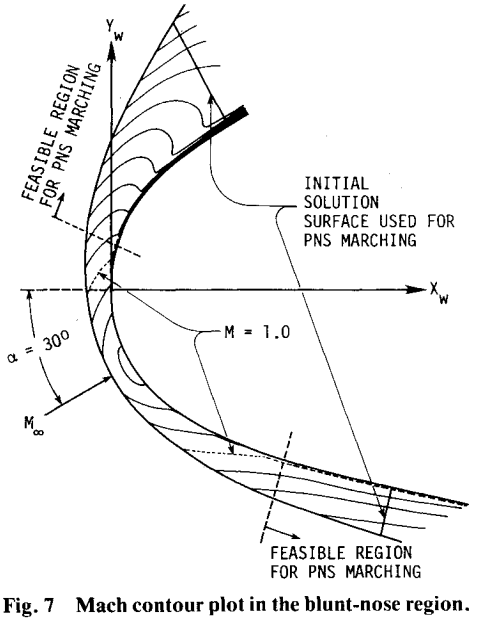

Fig. 7 Mach contour plot in the blunt-nose region.

For the 0-deg angle-of-attack case, the axisymmetric code of Ref. 30 was used to calculate the blunt-nose region. Because of the axisymmetric shape of the blunt-nose region, the required starting solution for the generalized PNS code was readily obtained in this case.

Results

The generalized PNS code has been used to compute the laminar flow around the forward half of the Space Shuttle Orbiter. Two different flow conditions were chosen and the results are compared with available experimental data.

The flow conditions corresponding to the first case are $M_\infty = 4.6$, $\alpha = 0$ deg, $Re_L = 0.129 \times 10^7$, $T_\infty = 67.32$ K, and $p_\infty = 0.4556 \times 10^3$ N/m^2 with an adiabatic wall boundary condition. Using these initial conditions, the solution for the

blunt-nose region was obtained with the axisymmetric time-dependent code.[30] The Space Shuttle Orbiter nose region consists of a spherical nose segment that subtends on angle of 45 deg at the sphere center, followed by a small conical segment which extends up to 10 in. from the nose. The axisymmetric computations were performed for a sphere-cone body with 26 grid points along the body and 31 grid points normal to the body.

The PNS computation was started with the initial solution obtained from the time-dependent code at the end of the conical section. The PNS solution was marched downstream and the solution surfaces were rotated slowly from the initial solution surface to an axis-normal plane at $x/L=0.125$. More grid points were added to the computation as it proceeded downstream. At an axial location of $x/L=0.2$ the grid contained 45 grid points around the body and 41 grid points normal to the body. The space marching was continued to an axial location of $x/L=0.48$.

Figure 4 shows the surface pressure coefficient comparison between the computed results and the experimental data[31] in the $\phi=0$ deg plane. In Fig. 5, the lee side ($\phi=180$ deg) surface pressure coefficients are compared. The agreement with the experiment is very good on both the wind and lee sides. Figure 6 shows the cross-flow velocity vector directions at $x/L=0.36$. The development of the complex flowfield around the Shuttle geometry is clearly visible. At 0 deg angle of attack, the windward side ($\phi=0$ deg plane) is at a lower pressure than the $\phi=180$ deg side and the streamlines from the lee side curve toward the wind side. As the wing starts to protrude from the fuselage, a vortex develops near the wing-body juncture and changes the local flow pattern.

The flow conditions corresponding to the second case are $M_\infty=7.9$, $\alpha=30$ deg, $Re_L=0.215\times10^7$, $T_\infty=52.33$ K, $p_\infty=72.95$ N/m^2, and $T_w=294.6$ K. The time-dependent blunt-body code was used to calculate the blunt-nose solution in the wind-axis coordinate system. A $31\times31\times21$ grid was used in the calculation. Figure 7 shows the sonic line on the wind and lee sides as well as the initial solution surface for the PNS solver. The initial solution surface and the solution vectors were rotated from the wind-axis system to the body-axis system and the PNS solver was marched downstream. The solution surfaces were rotated slowly from the initial orientation to an x-axis normal plane at $x/L=0.20$. Solutions up to $x/L=0.48$ were obtained with the PNS code.

Figure 8 compares the computed shock shape for the above flow conditions with the experimental[32] shock shape at $M_\infty=7.4$. The Mach number difference between the experiment and the computations has very little effect on the shock shape or the surface pressure coefficient profiles. Due

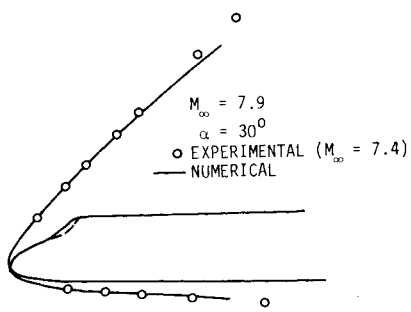

Fig. 8 Shock shape comparison.

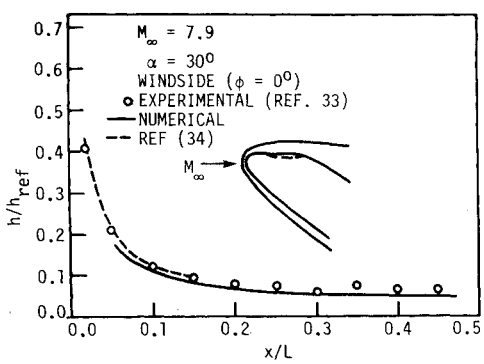

Fig. 9 Heat-transfer comparison on wind side.

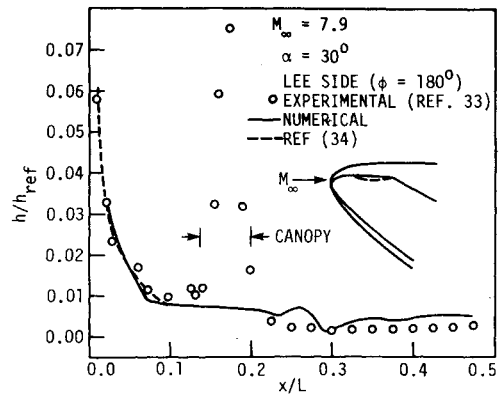

Fig. 10 Heat-transfer comparison on lee side.

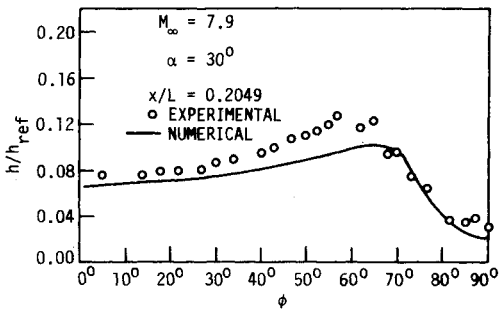

Fig. 11 Heat-transfer comparison at $x/L=0.205$.

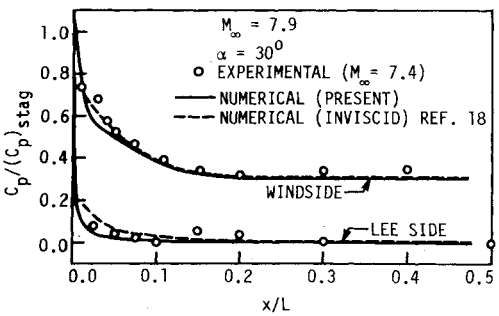

Fig. 12 Wall pressure comparison.

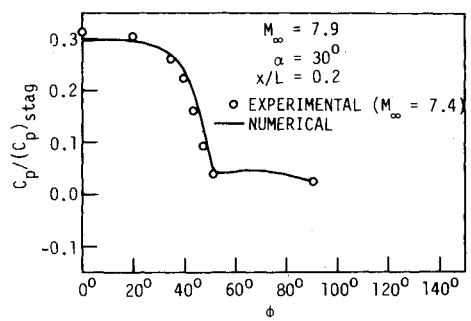

Fig. 13 Wall pressure comparison at $x/L=0.2$.

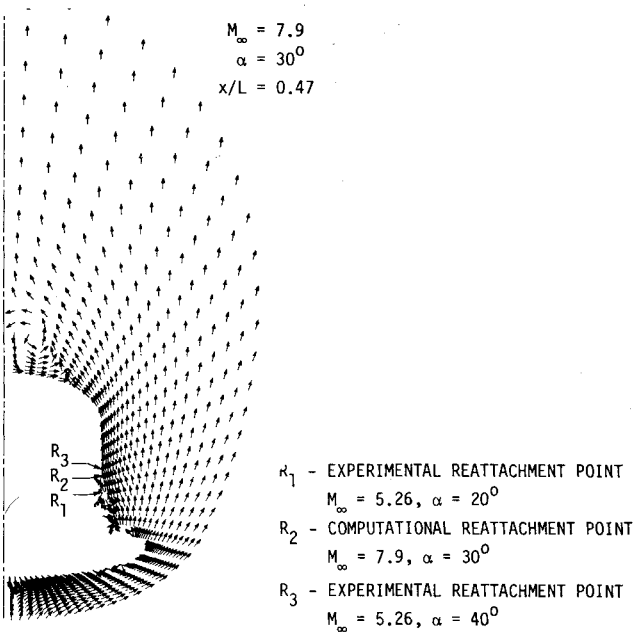

Fig. 14 Cross-flow velocity vector directions at $x/L = 0.47$.

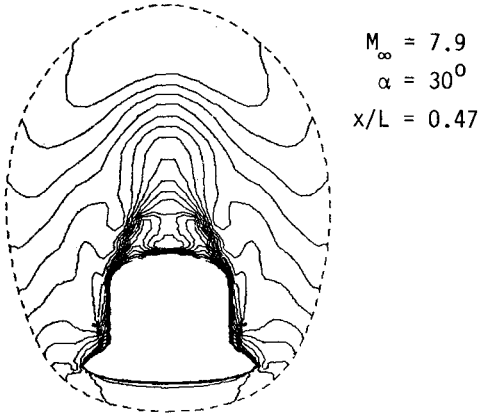

Fig. 15 Mach number contours at $x/L = 0.47$.

to the presence of the canopy, a canopy shock developed in the experiment and changed the outer shock shape on the lee side. As a result, the computational shock shape on the lee side is slightly different from the experimental shock shape downstream of the canopy region.

Figures 9 and 10 show the heating distribution on the windward and leeward sides in the plane of symmetry. There is reasonably good agreement with experiment[33] and with boundary-layer computations[34] except in the canopy region on the leeward side. As mentioned previously, the canopy was not included in the present computations.

In Fig. 11, the circumferential heating at $x/L = 0.205$ is compared with experiment, again with reasonably good agreement. The peak heating at $\phi \simeq 60$ deg is underpredicted by about 20%, however. This could be due to a lack of resolution of the computational grid near the body chine where the curvature is large.

Figure 12 compares the pressure distribution in the plane of symmetry with experiment and the inviscid computations of Li.[18] The agreement is excellent. Note that the canopy region was not resolved in the experiment, and was not modeled by either computation. The experiment was at $M_\infty = 7.4$, while the present computations were done at $M_\infty = 7.9$. This Mach number difference has a negligible effect on the pressure coefficient. The circumferential pressure distribution at

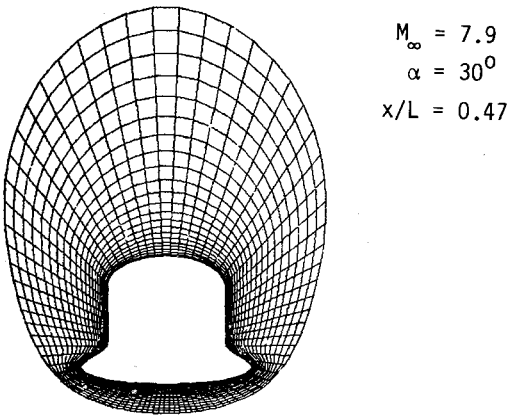

Fig. 16 Grid at $x/L = 0.47$.

$x/L = 0.2$ is shown in Fig. 13, and agreement with experiment is excellent.

In Fig. 14 the cross-flow velocity vector directions at $x/L = 0.47$ show the presence of two vortices, one on the lee side and the other near the wing-body juncture. Experimental oil-flow studies indicate the reattachment point at $x/L = 0.47$ to be close to the location predicted by the present computations. The local grid structure may play a very important role in resolving the vortex structure in that region. Figure 15 shows the Mach number contours at $x/L = 0.47$ and Fig. 16 shows the grid structure at the same axial location.

The present results were obtained on a CDC 7600 computer. The generalized PNS code required 1.8×10^{-3} s/grid point/step. A typical PNS solution at 30 deg angle of attack took around 400 steps and 20 min. The blunt-body code, on the other hand, required 3.5 h of CPU time to converge the solution in the blunt-nose region.

Concluding Remarks

The generalized PNS code and the time-dependent blunt-body code have been used successfully to compute the complete flow around the Space Shuttle Orbiter forebody at two different flow conditions. The good agreement between the computational results and the experimental data proves the effectiveness of the generalized PNS solver. The complex flow structure that develops near the wing-body region is predicted reasonably well by the generalized PNS solver. It is believed that an improved grid will permit the computation to continue to the aft portion of the Shuttle.

Computation of the wing region should be possible if the flow outside of the boundary layer is supersonic, and there is evidence that this is the case. Regions of reversed axial flow remain a problem for the present code, and this is expected only on the canopy, which was streamlined in the present computations.

Acknowledgments

This work was supported by NASA Ames Research Center under Grant NGR 16-002-038 and the Computational Fluid Dynamics Institute, Iowa State University, Ames, Iowa. The authors wish to acknowledge the helpful suggestions given by Drs. Rizk and Chaussee in obtaining the blunt-body solution.

References

[1] Rubin, S. G. and Lin, T. C., "Numerical Methods for Two- and Three- Dimensional Viscous Flow Problems: Application to Hypersonic Leading Edge Equations," Polytechnic Institute of Brooklyn, Farmingdale, N.Y., PIBAL Rept. 71-8, April 1971.

[2] Lin, T. C. and Rubin, S. G., "Viscous Flow Over a Cone at Moderate Incidence: I. Hypersonic Tip Region," *Computers and Fluids,* Vol. 1, Feb. 1973, pp. 37-57.

[3] Lubard, S. C. and Helliwell, W. S., "Calculation of the Flow on a Cone at High Angle of Attack," *AIAA Journal,* Vol. 12, July 1974, pp. 965-974.

[4]Lubard. S. C. and Rakich, J. V., "Calculation of the Flow on a Blunted Cone at a High Angle of Attack," AIAA Paper 75-149, Jan. 1975.

[5]Rakich, J. V. and Lubard, S. C., "Numerical Computation of Viscous Flows on the Lee Side of Blunt Shapes Flying at Supersonic Speeds," *Proceedings of the NASA Conference on Aerodynamic Analyses Requiring Advanced Computers,* NASA SP-347, March 1975, pp. 531-542.

[6]Vigneron, Y. C., Rakich, J. V., and Tannehill, J. C., "Calculation of Supersonic Viscous Flow over Delta Wings with Sharp Subsonic Leading Edges," AIAA Paper 78-1137, July 1978.

[7]Schiff, L. B. and Steger, J. L., "Numerical Simulation of Steady Supersonic Viscous Flow," *AIAA Journal,* Vol. 18, Dec. 1980, pp. 1421-1430.

[8]Tannehill, J. C., Venkatapathy, E., and Rakich, J. V., "Numerical Solution of Supersonic Viscous Flow over Blunt Delta Wings," *AIAA Journal,* Vol. 20, Feb. 1982, pp. 203-210.

[9]Rakich, J. V. and Kutler, P., "Comparison of Characteristics and Shock Capturing Methods with Application to the Space Shuttle Vehicle," AIAA Paper 72-191, Jan. 1972.

[10]Kutler, P., Lomax, H., and Warming, R. F., "Computation of Space Shuttle Flowfields Using Noncentered Finite-Difference Schemes," *AIAA Journal,* Vol. 11, Feb. 1973, pp. 196-204.

[11]Moretti, G., Grossman, B., and Marconi, F. Jr., "A Complete Numerical Technique for the Calculation of the Three-Dimensional Inviscid Supersonic Flows," AIAA Paper 72-192, Jan. 1972.

[12]Marconi, F. and Salas, M., "Computation of Three Dimensional Flows About Aircraft Configurations," *Computers and Fluids,* Vol. 1, June 1973, pp. 185-195.

[13]Marconi, F., Yaeger, L., and Hamilton, H. H., "Computation of High Speed Inviscid Flows about Real Configurations," *Proceedings of the NASA Conference on Aerodynamic Analyses Requiring Advanced Computers,* NASA SP-347, March 1975, pp. 1411-1455.

[14]Chaussee, D. S. and Kutler, P., "Inviscid Supersonic/Hypersonic Body Flowfield and Aerodynamics from Shock-Capturing Technique Calculations," *Journal of Spacecraft and Rockets,* Vol. 13, June 1976, pp. 325-331.

[15]Rakich, J. V. and Lanfranco, M. J., "Numerical Computation of Space Shuttle Laminar Heating and Surface Streamlines," *Journal of Spacecraft and Rockets,* Vol. 14, May 1977, pp. 265-272.

[16]Goodrich, W. D., Li, C. P., Houston, C. K., Chiu, P., and Olmedo, L., "Numerical Computations of Orbiter Flowfields and Laminar Heating Rates," *Journal of Spacecraft and Rockets,* Vol. 14, May 1977, pp. 257-264.

[17]Li, C. P., "Implicit Solution for the Shock-Layer Flow Around General Bodies," *AIAA Journal,* Vol. 20, Feb. 1982, pp. 175-183.

[18]Li, C. P., "Numerical Simulation of Reentry Flow Around the Shuttle Orbiter Including Real Gas Effects," *Computers in Flow Predictions and Fluid Dynamics Experiments,* Nov. 1981, pp. 141-145.

[19]Lighthill, M. J., "On Boundary Layers and Upstream Influence. II. Supersonic Flow Without Separation," *Proceedings of the Royal Society, Series A,* Vol. 217, pp. 478-507.

[20]Lindemuth, I. and Killeen, J., "Alternating Direction Implicit Techniques for Two Dimensional Magnetohydrodynamics Calculations," *Journal of Computational Physics,* Vol. 13, Oct. 1973, pp. 181-208.

[21]McDonald H. and Briley, W. R., "Three-Dimensional Supersonic Flow of a Viscous or Inviscid Gas," *Journal of Computational Physics,* Vol. 19, Oct. 1975, pp. 150-178.

[22]Beam, R. and Warming, R. F., "An Implicit Factored Scheme for the Compressible Navier-Stokes Equations," *AIAA Journal,* Vol. 16, April 1978, pp. 393-401.

[23]Venkatapathy, E., Rakich, J. V., and Tannehill, J. C., "Numerical Solution of Space Shuttle Orbiter Flowfield," AIAA Paper 82-0028, Jan. 1982.

[24]Thomas, P. D., Vinokur, M., Bastianon, R. A., and Conti, R. J., "Numerical Solution for Three-Dimensional Inviscid Supersonic Flows," *AIAA Journal,* Vol. 10, July 1972, pp. 887-894.

[25]Kutler, P., Reinhardt, W. A., and Warming, R. F., "Multishocked Three-Dimensional Supersonic Flowfields with Real Gas Effects," *AIAA Journal,* Vol. 11, May 1973, pp. 657-664.

[26]Myers, R. M., "Users Guide for a Three-Dimensional Aircraft Body Fit Program," Lockheed Electronics Co., Houston, Tex., Tech. Memo. 5060, 1975.

[27]Kutler, P., Pedelty, J. A., and Pulliam, T. H., "Supersonic Flow over Three-Dimensional Ablated Nosetips Using an Unsteady Implicit Numerical Procedure," AIAA Paper 80-0063, Jan. 1980.

[28]Rizk, Y. M., Chaussee, D. S., and McRae, D. S., "Computation of Hypersonic Viscous Flow Around Three-Dimensional Bodies at High Angles of Attack," AIAA Paper 81-1261, June 1981.

[29]Rizzi, A. and Bailey, H., "Reacting Nonequilibrium Flow Around the Space Shuttle Using a Time Split Method," *Proceedings of the NASA Conference on Aerodynamic Analyses Requiring Advanced Computers,* NASA SP-347, March 1975, pp. 1327-1349.

[30]Tannehill, J. C., Holst, T. L., and Rakich, J. V., "Numerical Computation of Two-Dimensional Viscous Blunt Body Flows with an Impinging Shock," *AIAA Journal,* Vol. 14, Feb. 1976, pp. 204-211.

[31]Kingsland, R. B., "Aeroheating (Pressure) Characteristics on a 0.010-scale Version of the Vehicle 3 Space Shuttle Configuration," NASA CR-144608, Vol. 1, May 1976.

[32]Dye, W. H. and Polek, T., "Results of Pressure Distribution Tests of a 0.01-scale Space Shuttle Orbiter Model in the NASA/ARC 3.5 Foot Hypersonic Wind Tunnel (Test OH38)," NASA CR-144584, Dec. 1975.

[33]Dye, W. H., "Aerodynamic Heating Results Obtained During Test OH50B Conducted in the AEDC VKF Tunnel B Using the 0.040-scale Model 83-0 of the Space Shuttle Orbiter Forward Fifty Percent Fuselage," NASA CR-151067, June 1977.

[34]Lanfranco, J. M., "Critical Evaluation of a Method for Space Shuttle Heat Transfer and Surface Streamline Predictions," Informatics-PMI, Inc., Palo Alto, Calif., TN-1335-44-1, Oct. 1976.